

Magnetoresistance and magnetization reversal of single Co nanowires

R. A. Silva, T. S. Machado, G. Cernicchiaro, A. P. Guimarães, and L. C. Sampaio
Centro Brasileiro de Pesquisas Físicas, Rua Dr. Xavier Sigaud, 150, Rio de Janeiro 22.290-180, RJ, Brazil
 (Received 23 December 2008; revised manuscript received 26 March 2009; published 29 April 2009)

The magnetization reversal in Co single wires was investigated through magnetoresistance measurements and micromagnetic simulations. We developed a model to calculate the magnetoresistance based on the magnetization structure obtained by the solution of the Landau-Lifshitz-Gilbert equation. It allowed us to understand details of the magnetoresistance curves, including the jumps that are related to the magnetization reversal process. Depending on the angle between the wire and the applied magnetic field, simulations show that the magnetization structure exhibits curling or uniform rotation modes in the magnetization reversal process. In the curling mode, the magnetization structure exhibits a vortex along the wire with its core displaced from the wire axis. For angles larger than 50° the vortex core is close to the wire surface and disappears at 80° , changing the mode from curling to uniform rotation. Our model for computing the magnetoresistance revealed to be a useful tool in the understanding of magnetic properties of nanostructures.

DOI: [10.1103/PhysRevB.79.134434](https://doi.org/10.1103/PhysRevB.79.134434)

PACS number(s): 75.60.-d

I. INTRODUCTION

Recently, the search for new kinds of electronic devices using nanowires has attracted a huge interest. Among the main motivations one can cite, for instance, the shrinking of the electronic circuits, new functionalities such as optoelectronics,¹ and applications as sensor elements.² Probably, nanowires are emerging as building blocks for a new generation of nanoelectronic devices.³ Other applications have been proposed which take into account spin transfer effects. Within certain conditions the domain wall movement can be controlled by a spin polarized current, a property that can be used either to create a nonvolatile memory⁴ or to perform logical operations.⁵

The magnetization reversal in individual small particles and nanowires has been discussed for a long time. Studies based on magnetic measurements of such small objects are difficult to be performed due to the tiny magnetic signal. Only a few results were reported so far using microsuperconducting quantum interference device (micro-SQUID) magnetometry⁶ and magnetic force microscopy (MFM).⁷ An alternative approach to probe the magnetic properties of nanowires consists of the measurement of the electronic transport in the presence of a magnetic field. The magnetoresistance, mainly the anisotropic magnetoresistance (AMR), is very sensitive to small changes in the magnetization and has become a useful tool to study the magnetization reversal in nanowires⁸⁻¹² and in other nanoscale systems.

In this paper we explore by experiments and numerical simulations the magnetization reversal in Co nanowires. We have calculated the magnetic structure for a single Co nanowire by micromagnetic modeling and the corresponding magnetoresistance. The focus of this work is to discuss whether the magnetization reversal occurs by curling, by uniform rotation, or by a wall displacement in the limit of long wire and the relationship between these magnetization reversal modes with the magnetoresistance. The model developed to calculate the magnetoresistance revealed to be a useful tool to understand details of the magnetoresistance experimental curves. As we shall see, the existence of vortices in

the magnetization reversal explains the observed behavior in the experiments. The paper is organized as follows. First, in Sec. II the nanowire preparation and the electric transport measurements in single nanowires are detailed. Section III describes the model to simulate the magnetic structure and to calculate the magnetoresistance, taking into account the local magnetization. In the remaining sections, the results obtained from the experiments and simulations are discussed.

II. EXPERIMENT

Co wires were grown by electrodeposition using porous polycarbonate membranes as template. The membranes are metalized on both sides with a Au film; in one side the film is thick enough (300 nm) to close the pores and on the other side the film is relatively thin (50 nm) keeping the pores open. The membranes are positioned in front of the counter-electrode (CE) with the thicker Au film on the backside of the membrane, which acts as working electrode (WE) (see Fig. 1). A potential difference of -1 V between WE and CE electrodes is applied, measured in relation to the Ag/AgCl reference. We have used membranes commercialized by GE Water & Process.¹³ The solution used in the electrodeposi-

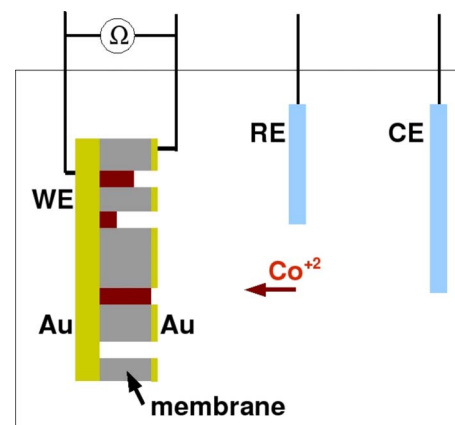


FIG. 1. (Color online) Scheme of the wire growth process.

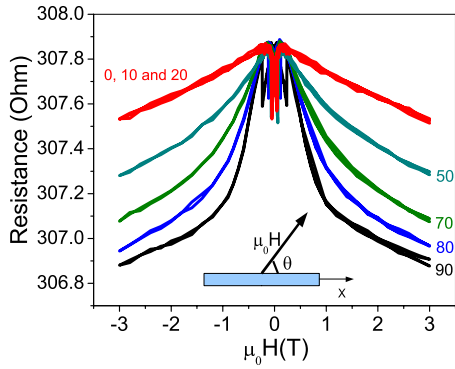


FIG. 2. (Color online) Magnetoresistance measurements of a single Co wire with diameter of 50 nm and 6 μm long varying the angle between the magnetic field and the wire from 0° to 90° .

tion was constituted of 120 g/l of CoSO_4 and 30 g/l of H_3BO_3 with pH 4. The wire growth process takes some 70 s. For more details on the sample preparation see Ref. 14.

To follow the wire growth process inside the pores, we measure the resistance between the two sides of the membrane (see Fig. 1). The instant when the resistance drops corresponds to the electrical contact of just one or a few wires that touch the thin Au film, and the growth is stopped. This process can also be monitored measuring the electrodeposition current. Such fast decrease in the resistance is accompanied by a fast increase in the electrodeposition current. Through this process, it is possible to obtain an electrical contact from a single wire. We have obtained a success rate of one in three trials to get a good electrical contact. The membranes are fixed in a sample holder and after the wire growth process is finished, the sample is immediately placed in a cryostat for electric transport measurements. Inside the cryostat, the electric contact remains for months, even after cycling the temperature between 4 K and room temperature for several times, but at room atmosphere the contacts open in 1–2 days.

The wires have a diameter of 50 nm and are 6 μm long. These dimensions lead to an aspect ratio of 1:120 which allows us to compare our results with predictions expected in the limit of an infinite wire. The resistance measured for a single wire is 300 Ω approximately, and if two or three wires are connected, this value decreases to half or one-third, respectively.

We have measured the magnetoresistance of single Co wires at 300 K. The wires are rotated in relation to the magnetic field direction allowing to probe the dependence of the magnetoresistance with the angle (θ) between the field and the current (or the wire), as it is shown in the inset of Fig. 2. Figure 2 shows the magnetoresistance as the angle θ varies from 0° to 90° . It is interesting to remark the good quality of signal-to-noise ratio obtained. The curves show the raw data; no correction was performed. Since the pores are only approximately perpendicular to the membrane surface and the membrane is itself mechanically flexible, the value of θ is not precise and one has to consider an angle of 2° – 3° as an error bar.

The magnetoresistance exhibits jumps at low fields as can be seen from Fig. 2 and in detail in Fig. 3 for $\theta=20^\circ$ and 80° .

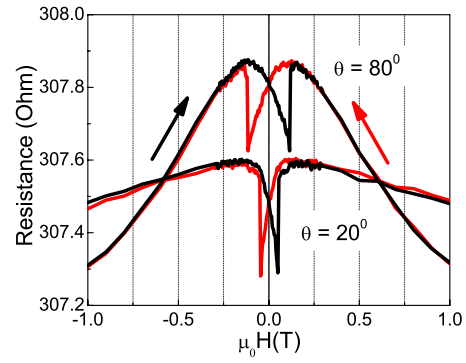


FIG. 3. (Color online) Magnetoresistance measurements for $\theta = 20^\circ$ and 80° . For the sake of clarity, for 20° the curve was shifted downward by 0.22 Ω . Black and red curves correspond to different senses of sweeping field.

Red and black lines illustrate the sense of sweeping field. The jumps occur at a field known as switching field (H_{SW}). H_{SW} is almost constant for low θ values and increases fast close to 90° (see Fig. 4). The angles 20° and 80° were chosen to be representative of each range, i.e., small and large θ , respectively.

III. THEORETICAL APPROACH

To better understand the experimental results we have developed a model to calculate the magnetoresistance. One of the most important points of the model is to consider the magnetization structure along the wire with all inhomogeneities that can occur for any applied magnetic field. To do so, we have first calculated the magnetization structure by solving the Landau-Lifshitz-Gilbert (LLG) equation for a Co wire with the same dimensions as in the experiments. Beside the magnetoresistance, we have calculated the magnetic hysteresis cycle and the dependence on θ of the switching field.

A. Micromagnetic calculations

The LLG equation is given by

$$\frac{d\mathbf{m}}{dt} = -\gamma_0 \mathbf{m} \times \mathbf{H}_{\text{eff}} + \alpha \mathbf{m} \times \frac{d\mathbf{m}}{dt}, \quad (1)$$

where γ_0 is the gyromagnetic ratio, \mathbf{m} is the normalized magnetization, and \mathbf{H}_{eff} is the total magnetic field, including

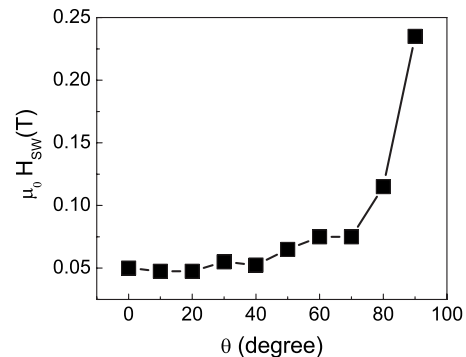


FIG. 4. Dependence of the switching field on θ . The line is a guide for the eyes.

the external applied field and the dipolar field. We used the typical magnetic parameters of Co: the saturation magnetization is $M_s = 1400 \times 10^3$ A/m, the exchange coupling is $A = 30 \times 10^{-12}$ J/m, and the Gilbert damping constant is $\alpha = 0.2$. The only source of magnetic anisotropy is the shape anisotropy; the magnetocrystalline anisotropy was not considered. We have simulated Co wires with the cross section of 50×50 nm² and length of 6 μ m.

Even though the wires used in experiments are cylinders, the use of a square cross section in simulations does not alter the comparison between experiments and simulations. We used a hexagonal cross section as well and almost identical results were found. The wire is discretized in cells of $5 \times 5 \times 5$ nm³. This cell size is very close to the exchange length of Co ($\sqrt{2A/\mu_0 M_s^2} \approx 4.9$ nm) which ensures that within this volume the magnetization is homogeneous as it is needed in micromagnetic simulations.¹⁵ We have developed our own code. Besides the magnetization structure the code calculates the magnetization dynamics under the action of pulses of magnetic field or spin polarized current.¹⁶ To obtain the hysteresis cycle the magnetization is calculated for a fixed field during a time necessary to reach a quasiequilibrium state. After that the field is changed and a new calculation is performed. This is repeated for different fields between negative and positive saturation fields, thus completing the cycle.

B. Model for the magnetoresistance

The AMR is the source of the observed magnetoresistance. Applying a magnetic field on the θ direction, the resistivity for a monodomain magnet is given by

$$\rho = \rho_{\perp} + (\rho_{\parallel} - \rho_{\perp}) \cos^2 \phi, \quad (2)$$

where ρ_{\perp} and ρ_{\parallel} are the resistivities when the magnetization is pointing perpendicular or parallel to the wire axis, respectively.¹⁷ ϕ is the angle between the magnetization and the wire (or direction of the electrical current). The projection of the total magnetization (M_x) on the wire is $M_x = M_s \cos \phi$, or taking the normalized projection $m_x = \cos \phi$, and Eq. (2) is rewritten as

$$\rho = \rho_{\perp} + (\rho_{\parallel} - \rho_{\perp}) m_x^2. \quad (3)$$

To calculate the magnetoresistance curves considering the inhomogeneities of the magnetization, one takes Eq. (3) considering now m_x as the magnetization of a cell i used in the micromagnetic simulations. Thus, the contribution of each cell is given by

$$\rho_i = \rho_{i,\perp} + (\rho_{i,\parallel} - \rho_{i,\perp}) m_{x,i}^2. \quad (4)$$

In order to calculate the total wire resistance, ρ_i is transformed in the local resistance $R_i = \rho_i L_i / A_i$, where L_i ($=5$ nm) and A_i ($=5 \times 5$ nm²) are the length and cross section area of the cell, respectively. The magnetoresistance [$R(H)$] is then obtained calculating the equivalent resistance as a function of the applied field. Notice that $m_{x,i}$ changes with the field, which is obtained by solving the LLG equation.

The wires have in the cross section 10×10 cells. Since the cross section does not change along the wire, one can

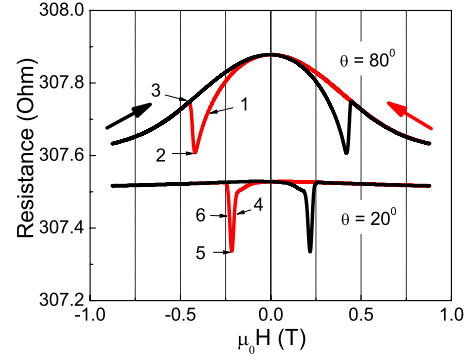


FIG. 5. (Color online) Magnetoresistance calculated for 20° and 80°. The curve of 20° was shifted downward by 0.35 Ω . Black and red curves correspond to different sweep field directions.

consider the wire as composed by lines, 10×10 lines, each line with 1200 ($=6000$ nm/5 nm, wire length/cell size) cells. The equivalent resistance of the wire is then computed taking the cells in the line as being resistances in series and the lines as being resistances in parallel. With such configuration, the total or equivalent wire resistance is straightforwardly calculated.

IV. DISCUSSION

A. Magnetoresistance

In order to calculate the magnetoresistance using Eq. (4), i.e., expressed in terms of resistance, we have to obtain previously R_{\perp} and $R_{\parallel} - R_{\perp}$. These values are obtained from the experiments. R_{\perp} is given by the resistance value for which $m_x = 0$ and R_{\parallel} when the applied field is at saturation, i.e., $m_x = 1$. To obtain R_{\perp} , as it will be shown later, the field where m_x is null is easily identified. For R_{\parallel} we have to take into account the slope at high fields in the experimental magnetoresistance curves and remove it. For the wire R_{\perp} and $R_{\parallel} - R_{\perp}$ are 307.8 and 0.3 Ω , respectively. In the calculations, for the cells one has to consider the geometrical factors and one finds $R_{i,\perp}$ and $R_{i,\parallel} - R_{i,\perp}$ equal to 307.8/12 and 0.3/12 Ω , respectively. Figure 5 shows the magnetoresistance calculated for $\theta = 80^\circ$ and 20° .

The curves obtained by simulations exhibit a good agreement with experimental measurements; notice that one used the same scale of the experimental resistance measurements (see Fig. 3). A difference, however, is observed for the H_{SW} values. This happens because simulations do not take into account the temperature; actually they correspond to calculations for the low temperature limit. Furthermore, in experiments the wires have defects that contribute to decrease H_{SW} . These are some reasons for the larger H_{SW} values found in simulations. We are actually interested in the qualitative agreement between results obtained from experiments and simulations.

B. Magnetization reversal

The good agreement between experiments and simulations in the magnetoresistance curves has motivated us to explore what happens to the wire magnetization on the mag-

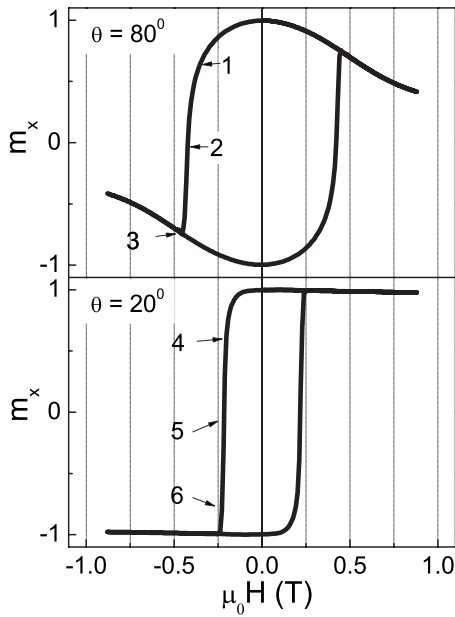


FIG. 6. Hysteresis curves along the wire axis (m_x) calculated for 20° and 80° .

magnetization reversal. Figure 6 shows the wire magnetization component m_x varying the magnetic field, with the same parameters used in the data shown in Fig. 5. This component is obtained through the summation $\sum m_{x,i}/N$ over all N cells. It is worth noticing the agreement between the calculated magnetization with experimental results obtained by micro-SQUIDS for a single wire for small and large angles (see Fig. 2 of Ref. 6).

As can be seen from Fig. 6, the magnetization curves are quite similar except by the approach to the saturation and the H_{SW} values. It induces us to think that an identical magnetization reversal process should occur for both angle ranges.

Let us initially consider the dynamics of the magnetization reversal process for 80° . Starting from zero field and applying a negative field, the magnetization of the cells rotates at unison from the wire axis (0°) up to the critical angle (ϕ_{cri}) 90° and jumps to -135° [Fig. 7(a)] and continues to rotate up to be parallel to the applied field [Fig. 7(b)]. Notice that since the applied field is negative, it is indeed pointing along -100° .

Figures 7(c)–7(e) show the magnetization structures at the cross section, in the middle of the wire, on some points on the magnetization reversal in the magnetoresistance and magnetization curves. They correspond to the numbers “1,” “2,” and “3” shown in Figs. 5 and 6. Comparing the respective points in those curves, it is worth pointing out that the jump observed in the magnetoresistance from 2 to 3 does not correspond to the magnetization reversal from opposite magnetizations, such as 1 to 3 as should be expected. Actually, the jump from 2 to 3 occurs only after the magnetization reaches $m_x=0$, at ϕ_{cri} , that is, 90° .

A closer look into the magnetization structures shows that the magnetization is almost uniform before, after, and at the magnetization reversal, meaning that for $\theta=80^\circ$ as well as for large θ angles, the magnetization reversal process takes place through the uniform rotation process.

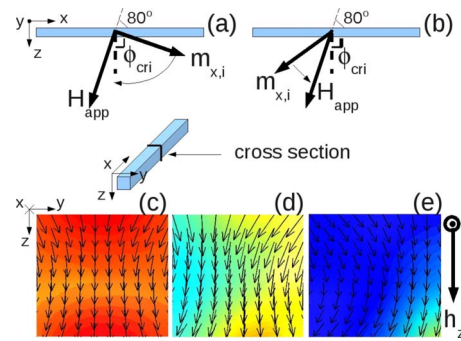


FIG. 7. (Color online) Magnetization from a lateral view of the wire for $\theta=80^\circ$ (a) before and (b) after the magnetization reversal. Below, snapshots of the magnetization at the middle of the wire (see inset). Red and blue colors correspond to $m_x=+1$ and -1 , respectively. (c)–(e) correspond to 1–3 positions shown in Figs. 5 and 6. The external arrow indicates the magnetic field direction.

For $\theta=20^\circ$, however, a different picture emerges. Close to H_{SW} the magnetization decreases and just before the reversal takes place the curling structure is formed, i.e., a vortex takes the entire wire with its core magnetized on the positive magnetization direction. Notice that the applied field is negative. This curling structure is formed at the same time along the wire; there is no wall nucleation and propagation in one of the ends of the wire. The core is displaced from the axis wire due to the h_z field component (see Fig. 8) which favors the magnetization region parallel to h_z . Figure 8 shows the magnetization structure at the cross section in the middle of the wire on some points in the magnetoresistance and magnetization curves (see numbers “4,” “5,” and “6” in Figs. 5 and 6). Just before the jump in the magnetoresistance that corresponds to the point 5, seen also in the experimental magnetoresistance curve (Fig. 3), one sees from the magnetization curve that this jump occurs only when $m_x=0$. It is even surprising because in the magnetoresistance measurements the magnetoresistance varies continuously until it attains the position 5 to jump subsequently. It is also interesting to remark that the vortex core remains with a positive magnetization on the entire demagnetization process; its magnetization decreases until it completely disappears when $m_x=-1$.

In order to analyze in more detail the mechanism of magnetization reversal we investigated the dependence of H_{SW} with the angle θ . In the limit of infinite wire the curling mode exhibits the following expression for H_{SW} :

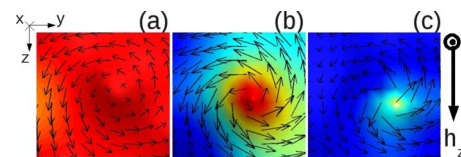


FIG. 8. (Color online) Magnetic structure for $\theta=20^\circ$ at the cross section in the middle of the wire. Red and blue colors correspond to $m_x=+1$ and -1 , respectively. (a)–(c) correspond to 4–6 positions shown in Figs. 5 and 6. The external arrow indicates the magnetic field direction.

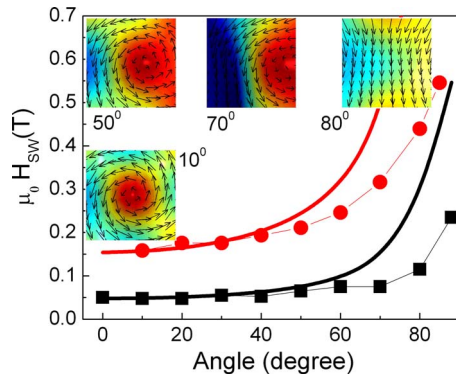


FIG. 9. (Color online) Switching field as a function of θ for experiments (square) and simulations (circle). The lines are the fittings using Eq. (5). For the inset, see text.

$$\mu_0 H_{SW} = \frac{\mu_0 M_s}{2} \frac{(a+1)a}{\sqrt{a^2 + (1+2a)\cos^2 \theta}}, \quad (5)$$

where $a = -1.08(d_0/d)^2$ with $d_0 = 5.2\sqrt{2A/\mu_0 M_s^2}$. From the seminal work of Treves and collaborators,^{18,19} in the limit of small θ , d_0 behaves as a critical value. For the wire diameter d smaller or larger than d_0 the magnetization reversal occurs via uniform rotation or curling, respectively. For the dimensions of our sample and using the respective A and M_s parameters, we found $d_0 \approx 25.5$ nm. Thus, since the wire diameter is 50 nm the switching process is expected to occur by the curling mode. Figures 4 and 9 (black square symbol) show the measured H_{SW} values for θ varying from 0° to 90° .

As pointed out by other authors the reversal process in wires takes place by curling and uniform rotation for small and large angles, respectively.¹¹ Our experimental data of H_{SW} , as well as the points obtained from simulations (red circle symbol), do not fit Eq. (5) in the range of large angles, as can be seen from Fig. 9; the lines are the best fittings of the points. However, for small angles the data are well fitted and the fitting of the experimental data provides $d_0 \approx 11$ nm, which is close to the calculated value. As mentioned before, the difference between the H_{SW} values obtained from experiments and simulations is intrinsic to the simulation method; it is used herein in a qualitative discussion.

An interesting question that we can have in mind is related to such change in magnetization reversal mode with θ . Let us examine the magnetization structure at the magnetization switching. Figure 9 shows, in the inset, the magnetization structures just before the switching for $\theta = 10^\circ$, 50° , 70° , and 80° . For 10° the curling mode is clearly observed with the vortex core close to the wire axis. Increasing θ , due to the larger H_{SW} value, the field component perpendicular to the wire also increases providing the displacement of the vortex core from the axis. Increasing θ once more, for 70° the vortex core is close to the wire surface. For 80° the vortex core is no longer present; it leaves the wire and the magnetization becomes almost uniform.

Such evolution on the magnetization structure with θ in the magnetization reversal allows us to unify the reversal process taking both small and large angle ranges. The magnetization reversal takes place by curling mode with the vortex core displaced from the axis wire. Increasing θ this effect is yet larger until the vortex core reaches the wire surface and disappears, changing thus the reversal mode to uniform rotation.

V. CONCLUSIONS

In conclusion, we presented the study of the magnetization reversal in single Co wires with dimensions in the limit of infinite wire through experiments and micromagnetic simulations. Based on the micromagnetic simulations, we developed a model to calculate the magnetoresistance and found a good agreement between simulations and the experimental results. Varying the angle θ between the wire and the applied field, the calculated magnetization structure in the magnetization reversal shows a continuous variation from curling to uniform rotation mode. It happens continuously through the displacement of the vortex core of the curling structure from the axis to the wire surface. It explains the reason for the appearance of two different modes of magnetization reversal.

ACKNOWLEDGMENTS

We thank J. E. Wegrowe and T. Wade for useful discussions on the sample preparation and T. G. Rappoport for helpful discussions. We acknowledge the Brazilian agencies CNPq and FAPERJ for financial support.

¹Y. Li, F. Qian, J. Xiang, and C. M. Lieber, *Mater. Today* **9**, 18 (2006).

²F. Patolsky, B. P. Timko, G. Zheng, and C. M. Lieber, *MRS Bull.* **32**, 142 (2007).

³N. J. Quitoriano and T. I. Kamins, *Nano Lett.* **8**, 4410 (2008).

⁴S. S. P. Parkin, M. Hayashi, and L. Thomas, *Science* **320**, 190 (2008).

⁵M. Hayashi, L. Thomas, R. Moriya, C. Rettner, and S. S. P. Parkin, *Science* **320**, 209 (2008).

⁶W. Wernsdorfer, B. Doudin, D. Mailly, K. Hasselbach, A.

Benoit, J. Meier, J. Ph. Ansermet, and B. Barbara, *Phys. Rev. Lett.* **77**, 1873 (1996).

⁷M. Lederman, R. O'Barr, and S. Schultz, *IEEE Trans. Magn.* **31**, 3793 (1995); R. O'Barr and S. Schultz, *J. Appl. Phys.* **81**, 5458 (1997); L. Belliard, J. Miltat, A. Thiaville, S. Dubois, J. L. Duvail, and L. Piroux, *J. Magn. Magn. Mater.* **190**, 1 (1998).

⁸J. E. Wegrowe, S. E. Gilbert, D. Kelly, B. Doudin, and J. P. Ansermet, *IEEE Trans. Magn.* **34**, 903 (1998); J. E. Wegrowe, D. Kelly, A. Franck, S. E. Gilbert, and J. P. Ansermet, *Phys. Rev. Lett.* **82**, 3681 (1999).

- ⁹L. Piraux, J. M. George, J. F. Despres, C. Leroy, E. Ferain, R. Legras, K. Ounadjela, and A. Fert, *Appl. Phys. Lett.* **65**, 2484 (1994); S. Pignard, G. Goglio, A. Radulescu, L. Piraux, S. Dubois, A. Declémy, and J. L. Duvaill, *J. Appl. Phys.* **87**, 824 (2000).
- ¹⁰R. Ferré, K. Ounadjela, J. M. George, L. Piraux, and S. Dubois, *Phys. Rev. B* **56**, 14066 (1997).
- ¹¹Y. Rheem, B. Y. Yoo, W. P. Beyermann, and N. V. Myung, *Nanotechnology* **18**, 125204 (2007); **18**, 015202 (2007); Y. Rheem, B. Y. Yoo, B. K. Koo, W. P. Beyermann, and N. V. Myung, *J. Phys. D* **40**, 7267 (2007).
- ¹²A. B. Oliveira, S. M. Rezende, and A. Azevedo, *Phys. Rev. B* **78**, 024423 (2008).
- ¹³GE Water & Process, Polycarbonate, 0.05 μm , KN5CP04700.
- ¹⁴T. L. Wade and J. E. Wegrowe, *Eur. Phys. J.: Appl. Phys.* **29**, 3 (2005).
- ¹⁵Jacques Miltat, Gonçalo Albuquerque, and Andre Thiaville, *Spin Dynamics in Confined Magnetic Structures I*, Topics Applied Physics 83 (Springer-Verlag, Berlin, 2002), pp. 1–34.
- ¹⁶T. S. Machado, T. G. Rappoport, and L. C. Sampaio, *Appl. Phys. Lett.* **93**, 112507 (2008).
- ¹⁷R. C. O’Handley, *Modern Magnetic Materials* (Wiley-Interscience, New York, 1999), Chap. 15.
- ¹⁸E. H. Frei, S. Shtrikman, and D. Treves, *Phys. Rev.* **106**, 446 (1957); S. Shtrikman and D. Treves, *J. Phys. Radium* **20**, 286 (1959).
- ¹⁹H. Kronmüller, in *General Micromagnetic Theory, Handbook of Magnetism and Advanced Magnetic Materials*, edited by H. Kronmüller and S. Parkin (Wiley, Chichester, 2007), Vol. 2, pp. 703–741.